A theoretical approach to the $O(^1D) + H_2O(X\,^1A_1)$ reaction: *Ab initio* potential energy surface and quasiclassical trajectory dynamics study

R. Sayós,[a] Carolina Oliva, and Miguel González[a]
Departament de Química Física i Centre de Recerca en Química Teòrica, Universitat de Barcelona,
Martí i Franquès, 1, 08028 Barcelona, Spain

An *ab initio* study of the ground potential energy surface (PES) of the $O(^1D) + H_2O$ system has been performed, employing Møller–Plesset methods. From the stationary and additional points calculated, the ground PES has been modeled as a triatomic system, with an OH group of the H_2O molecule treated as a single atom of 17.0 amu. The rate constant of reaction (1), $O(^1D) + H_2O \rightarrow 2OH$ (main reaction channel), estimated from the quasiclassical trajectory (QCT) calculations is reasonably close to the recommended experimental value. For the relative translational energies explored ($E_T = 0.234$, 0.303, and 0.443 eV) and H_2O at $T = 300$ K, the QCT OH vibrational populations are in good agreement with the experimental values reported for the new OH fragment, but the QCT OH average rotational energies are in general quite larger than the experimental ones. Regarding the stereodynamics, for $E_T = 0.234$ eV there is not a clear tendency to a particular rotational alignment of the OH product with respect to the initial relative velocity vector, in agreement with experiments. The QCT results also show that nearly all reactive trajectories leading to reaction (1) take place through an insertion microscopic mechanism, which, even at the highest E_T value considered (0.443 eV), is mainly (70%) a nondirect one. The collision complex has an average lifetime of about three rotational periods and a geometry around that of the HO(OH) hydrogen peroxide molecule. The QCT results concerning the microscopic mechanism of reaction (1) are in agreement with the suggested ones by the experimentalists to interpret their results. The present study should be considered as a starting point in the study of reaction (1) from which different aspects on the dynamics may be learned. © *2000 American Institute of Physics.* [S0021-9606(00)30840-6]
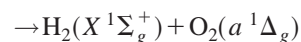
I. INTRODUCTION

The reactivity of the oxygen atom in the first excited electronic state, $O(^1D)$, is important in various fields of chemistry, and its reaction with water is relevant in stratospheric chemistry in the context of ozone degradation processes through the OH/HO_2 catalytic cycle.[1,2] The highly different reactive behavior of $O(^1D)$ with respect to the ground-state oxygen atom, $O(^3P)$, also makes the study of this kind of systems very interesting from a more fundamental point of view, to understand the origin of the different reactivities observed. Thus, the $O(^1D)$ atom is claimed to react very efficiently with compounds containing X–H bonds (such as H–H, C–H, O–H, and N–H), mainly through an insertion mechanism, while the analogous reactions with $O(^3P)$ present activation energy and occur by an abstraction mechanism.

The aim of this work is to study theoretically the gas phase reactions involved in the $O(^1D) + H_2O$ system, considering the ground potential energy surface (PES)

$$O(^1D) + H_2O(X\,^1A_1) \rightarrow 2\,OH(X\,^2\Pi)$$

$$\Delta H^0_{0K} = -28.9 \ \text{kcal mol}^{-1},^3 \qquad (1)$$

$$\rightarrow H_2(X\,^1\Sigma_g^+) + O_2(a\,^1\Delta_g)$$

$$\Delta H^0_{0K} = -24.8 \ \text{kcal mol}^{-1},^3 \qquad (2)$$

$$\rightarrow H(^2S) + HO_2(X\,^2A'')$$

$$\Delta H^0_{0K} = 5.6 \ \text{kcal mol}^{-1}.^3 \qquad (3)$$

Reaction (1) is known to be very fast, the thermal rate constant value approaching the gas kinetics value. The recommended rate constant value for reaction (1), $k(1)$, is $2.2(-0.45, +0.57) \times 10^{-10}$ cm^3 molecule^{-1} s^{-1} over the temperature range 200–350 K.[4] This result suggests that reaction (1) does not have activation energy, in contrast to what happens for the analogous reaction with $O(^3P)$, which has activation energy. At 298 K the $k(2)/k(1)$ ratio was found to be 0.01 (+0.005, −0.01),[5] and there is no information available on reaction (3). Hence, reaction (1) clearly corresponds to the main reaction of the $O(^1D) + H_2O$ system, accounting for around 99% of the reactivity at 298 K.

The nascent internal energy distribution of the OH radical has been measured in several experiments,[6–17] mainly involving the $^{16}O(^1D) + H_2\,^{18}O \rightarrow {}^{16}OH + {}^{18}OH$ reaction to differentiate between the new and old OH bonds formed,

using the laser induced fluorescence (LIF) technique. The reaction with D$_2$O has also been studied in some cases.[9,17] The O(^1D) atom has been generated by photodissociation of either N$_2$O ($\lambda = 193$ or 212.8 nm) or O$_3$ ($\lambda = 248$ or 266 nm). Therefore, OH($X\,^2\Pi$) rovibrational, spin–orbit, and lambda-doublet populations considering different O(^1D)+H$_2$O collision energy distributions have been determined experimentally. For the ^{16}OH molecule (new OH bond), vibrational populated levels up to $v'=2$ have been observed.[7,10] The vibrational and rotational distributions of the ^{18}OH molecule (old OH bond) have also been measured.[6,7,10,11,14] The ^{18}OH molecules are vibrationally and rotationally much colder than the ^{16}OH ones, nearly all of them being produced in $v'=0$. The OH spin–orbit population ratio ($X\,^2\Pi_{3/2}/X\,^2\Pi_{1/2}$) slightly deviates from the statistical expectation, and the lambda-doublet population ratio $[\Pi(A')/\Pi(A'')]$ exhibits some preference for the $\Pi(A')$ state.[10,11,14,17] Analogous studies to those reported for the bimolecular reaction (1) have also been reported for the corresponding photoinitiated half reaction from N$_2$O·H$_2$O,[15,17] N$_2$O·D$_2$O,[17] and O$_3$·H$_2$O[13] van der Waals complexes (H$_2\,^{18}$O in Refs. 13 and 15).

The stereodynamics of reaction (1) for the state-specific reaction channel leading to OH ($v'=2$, $N'=5$) has also been examined[16] using polarized Doppler-resolved LIF spectroscopy. The differential cross section (DCS) is nearly isotropic and the OH rotational angular momentum vector is predominantly perpendicular to both the initial and final relative velocity vectors. In addition, in a previous experiment[11] it has been shown that the ^{16}OH($v'=0,1$) molecule shows a negligible rotational alignment with respect to the initial relative velocity vector.

The above-mentioned experimental results regarding the internal energy distributions of ^{16}OH and ^{18}OH and the information about the stereodynamics are better explained considering that reaction (1) mainly takes place according to a microscopic mechanism which involves an HOOH collision complex formed by insertion of the O(^1D) atom into the H$_2$O molecule. The average lifetime of the collision complex should be of the order of the HOOH rotational period, and would not allow for a complete energy redistribution in the complex between the two resulting OH fragments.

Although there is a relatively large number of experimental studies reported on reaction (1), the corresponding theoretical information available is very limited. Thus, the theoretical studies are mainly devoted to the characterization of the PES around the hydrogen peroxide molecule[18–20] and OH+OH long-range[21] regions.

Because of the relevance of this system, and taking into account the very scarce theoretical information available on it, an *ab initio* characterization of the O(^1D)+H$_2$O ground PES has been performed in this work. Moreover, as a first approximation, a triatomic analytical representation of this PES has been derived, and a quasiclassical trajectory (QCT) dynamics study of reaction (1) has been performed. To the best of our knowledge, this contribution represents the first *ab initio* study carried out on the ground PES of the O(^1D)+H$_2$O system, taking into account all possible reactions, and

also the first theoretical study on the dynamics of reaction (1).

This work is organized as follows. Section II deals with the *ab initio* calculations and triatomic analytical fitting of the ground PES, and Sec. III shows the QCT dynamics study. In Sec. IV the summary and concluding remarks are given.

II. POTENTIAL ENERGY SURFACE

A. *Ab initio* calculations

For C_1 and C_s symmetries, the following PES correlate with the different asymptotic regions of reactions (1)–(3): (a) reactants $[\mathrm{O}(^1D)+\mathrm{H}_2\mathrm{O}(X\,^1A_1)]$:5 $^1A(C_1)$ and 3 $^1A' + 2\,^1A''(C_s)$; (b) products of reaction (1) $[\mathrm{OH}(X\,^2\Pi) + \mathrm{OH}(X\,^2\Pi)]$:4 $^1A + 4\,^3A(C_1)$ and 2 $^1A' + 2\,^1A'' + 2\,^3A' + 2\,^3A''(C_s)$; (c) products of reaction (2) $[\mathrm{H}_2(X\,^1\Sigma_g^+) + \mathrm{O}_2(a\,^1\Delta_g)]$:2 $^1A(C_1)$ and $^1A' + {}^1A''(C_s)$; (d) products of reaction (3) $[\mathrm{H}(^2S)+\mathrm{HO}_2(X\,^2A'')]$:$^1A + {}^3A(C_1)$ and $^1A'' + {}^3A''(C_s)$. Hence, all asymptotes may correlate adiabatically through a $^1A(C_1)$ or a $^1A''(C_s)$ PES. The C_1 symmetry is the most important one for theoretical studies on the dynamics of reactions that involve four or more atoms, but it will be seen at the end of this section that for this system most of the stationary points located on the ground PES have in general symmetries higher than C_1.

We have carried out an *ab initio* study of the ground PES (^1A) using the GAUSSIAN 94 package of programs.[22] The wave function associated with this system is mostly multireferent for the ground PES. Thus, in most of the PES regions the system behaves as an open-shell singlet, and only for arrangements close to the geometry of the closed-shell minima min 1 and H$_2$O$_2$ (hydrogen peroxide) and for the saddle point that connects both minima the wave function is single referent. Hence, the most suitable *ab initio* methods to study this PES are those which are multireferent, such as the second-order multiconfigurational perturbation theory (CASPT2) and multireference configuration interaction (MRCI) methods. But, although these *ab initio* methods are nowadays accessible for the characterization of PES stationary points, recent benchmark calculations with molecular correlated wave functions on simple triatomic reactions, such as F+H$_2$,[23,24] O+H$_2$,[24] and H+HCl,[24] have shown that only using very large wave functions and basis sets it is possible to achieve energy values close to the experimental data. This kind of high-level calculations are very expensive, especially when the characterization of a global PES involving a large number of electrons and atoms is desired. On the other hand, it has been shown that, under certain conditions, *ab initio* methods, such as the Møller–Plesset perturbational method, can reproduce quite satisfactorily the energetics of this kind of systems when the ''broken symmetry'' approach is considered.[25,26] In this context, the elimination of the spin contamination of the wave function becomes a critical aspect, as the use of the broken symmetry approach leads to energy values which lie between the triplet and singlet ones. An efficient projection algorithm[25] for the elimination of the spin contamination when Møller–Plesset perturbational methods are used is included in the GAUSSIAN 94 package.[22] However, although the single-point energy obtained using

TABLE I. Energetics of the system using different methods and basis sets.

Method	$E+ZPE$/kcal mol^{-1} [a,b]			
	$H_2O_2(X\ ^1A)$	$2\ OH(X\ ^2\Pi)$	$H_2(X\ ^1\Sigma_g^+)+O_2(a\ ^1\Delta_g)$	$H(^2S)+HO_2(X\ ^2A'')$
PUMP2(FC)//UMP2(FC)/6-311G(d,p)	−68.67(−71.88)	−22.72(−20.03)	−39.78(−34.51)	13.74(18.23)
PUMP2(FC)//UMP2(FC)/6-311G($2df,2pd$)	−71.43(−74.69)	−18.92(−16.28)	−40.49(−35.30)	15.11(19.56)
PUMP2(FC)//UMP2(FC)/6-311G($3d2f,3p2d$)	−71.72(−74.96)	−18.69(−16.12)	−38.34(−33.20)	16.82(21.25)
PUMP4(FU)/6-311G(d,p)//UMP2(FC)/6-311G($3d2f,3p2d$)	−72.40(−75.63)	−29.48(−26.91)	−31.83(−26.69)	9.28(13.71)
PUMP4(FU)/6-311G($2df,2pd$)//UMP2(FC)/ 6-311G($3d2f,3p2d$)	−76.38(−79.61)	−27.36(−24.79)	−31.53(−26.39)	9.48(13.90)
PUMP4(FU)//UMP2(FC)/6-311G($3d2f,3p2d$)	−77.45(−80.68)	−27.65(−25.08)	−29.99(−24.85)	10.27(14.70)
Experimental data	−78.3±0.1[c]	−28.9±0.6[c]	−24.8±0.1[c]	5.6±2.0[c]

[a]Energy referred to reactants. The theoretical values in parentheses correspond to the energy without including the UMP2 ZPE.
[b]Absolute values of energy (hartrees) for $O(^1D)+H_2O$ as a sum of fragments are: −151.142 944 [UMP2(FC)/6-311G(d,p)], −151.116 849 [PUMP2(FC)//UMP2(FC)/6-311G(d,p)], −151.218 893 [UMP2(FC)/6-311G($2df,2pd$)], −151.198 564 [PUMP2(FC)/UMP2(FC)/6-311G($2df,2pd$)], −151.238 708 [UMP2(FC)/6-311G($3d2f,3p2d$)], −151.219 137 [PUMP2(FC)//UMP2(FC)/6-311G($3d2f,3p2d$)], −151.172 934 [PUMP4(FU)/ 6-311G(d,p)//UMP2(FC)/6-311G($3d2f,3p2d$)], −151.262 176 [PUMP4(FU)/6-311G($2df,2pd$)//UMP2(FC)/6-311G($3d2f,3p2d$)], −151.286 242 [PUMP4(FU)//UMP2(FC)/6-311G($3d2f,3p2d$)].
[c]Reference 3 (ΔH_{0K}^0).

the broken symmetry approach can be corrected using this projection technique, the optimal geometries determined in this context are probably located between the singlet and the triplet ones.

Hence, we have selected as a suitable method of calculation the unrestricted second-order Møller–Plesset perturbation theory (UMP2) method using a large basis set [6-311G($3d2f,3p2d$) standard, 128 basis functions], and considering the frozen core (FC) approach (only valence electrons are correlated), UMP2(FC)/6-311G($3d2f,3p2d$) *ab initio* level hereafter, to characterize (geometry optimization and harmonic vibrational frequencies calculation) the stationary points of the ground PES. The energies of the stationary points and of the set of *ab initio* points required to obtain, as a first approximation, a triatomic analytical representation of the PES (Sec. II B) have been calculated at the spin-projected unrestricted fourth-order Møller–Plesset perturbation theory (PUMP4) method, using the same basis set as before but considering in this case the full electron (FU) approach (all electrons are correlated), PUMP4(FU)/ 6-311G($3d2f,3p2d$) *ab initio* level hereafter. The standard GAUSSIAN 94 option [MP4(SDTQ)] has been employed. The spin-projected method has been employed to eliminate large spin contaminations on the PES ($0.00<\langle S^2\rangle/\hbar^2<1.10$). In summary, the strategy used in the calculation of the PES has been the following: (a) first, the stationary points of the PES (reactants, products, saddle points, H_2O_2, and other minimum) have been optimized at the UMP2(FC)/ 6-311G($3d2f,3p2d$) level; (b) second, the connections [minimum energy paths (MEP) and mostly intrinsic reaction coordinate (IRC) calculations] between these stationary points have been calculated at the UMP2(FC)/ 6-311G($2df,2pd$); (c) finally, the energy of each point previously calculated at the UMP2(FC) level has been computed using the PUMP4(FU)/6-311G($3d2f,3p2d$) *ab initio* method. In the next paragraphs the present *ab initio* results will be compared with experimental data and previous *ab initio* calculations.

The energetics of the system using different methods and basis sets is shown in Table I, considering the H_2O_2 hydro-

gen peroxide minimum and the three different product asymptotes. No significant differences appear when the 6-311G($2df,2pd$) basis set is used instead of the larger 6-311G($3d2f,3p2d$) one. In fact, the methods selected here are the ones which best reproduce the exothermicity of the main reaction [reaction (1)] and predict the depth of the H_2O_2 minimum with 1% of deviation with respect to the experimental value. The results obtained for the geometries and harmonic frequencies of the H_2O, OH, H_2, $O_2(a\ ^1\Delta_g)$, and HO_2 reactant and product molecules using these methods also show a good agreement with experimental information. The $O(^1D)-O(^3P)$ and $O_2(a\ ^1\Delta_g)-O_2(X\ ^3\Sigma_g^-)$ energy splittings have only been described adequately at the PUMP4 level.

In what follows, the reported data correspond to the highest level calculation [PUMP4(FU)//UMP2(FC)/ 6-311G($3d2f,3p2d$)], and the energies are given, including the zero-point energy (ZPE), with respect to reactants, unless otherwise indicated. The geometries [UMP2(FC)] of the stationary points placed between reactants and products are plotted in Fig. 1, and the energies [PUMP4(FU)// UMP2(FC)], including the UMP2(FC) zero-point energies (ZPE), are indicated in Fig. 2. In this figure the different reaction pathways for reactions (1)–(3) are also shown schematically, where ''ts'' and ''min'' refer to the saddle points and minima, respectively. In Table II the harmonic vibrational frequencies [UMP2(FC)] of the stationary points are reported.

Reaction (1) can take place along two possible reaction pathways. The first one [insertion microscopic mechanism (via H atom migration)] involves the formation of products when the system evolves from reactants through the H_2O_2 hydrogen peroxide minimum, according to the following way: $O(^1D)+H_2O\rightarrow ts8\rightarrow min1\rightarrow ts9\rightarrow H_2O_2\rightarrow ts2\rightarrow OH +OH$. The saddle point ts8 explains the formation of min1 from reactants, and the second one (ts9) the formation of H_2O_2 from min1. The saddle point ts2 allows one to connect the hydrogen peroxide with the hydroxyl products. The saddle points ts8 and ts2, however, have only been obtained
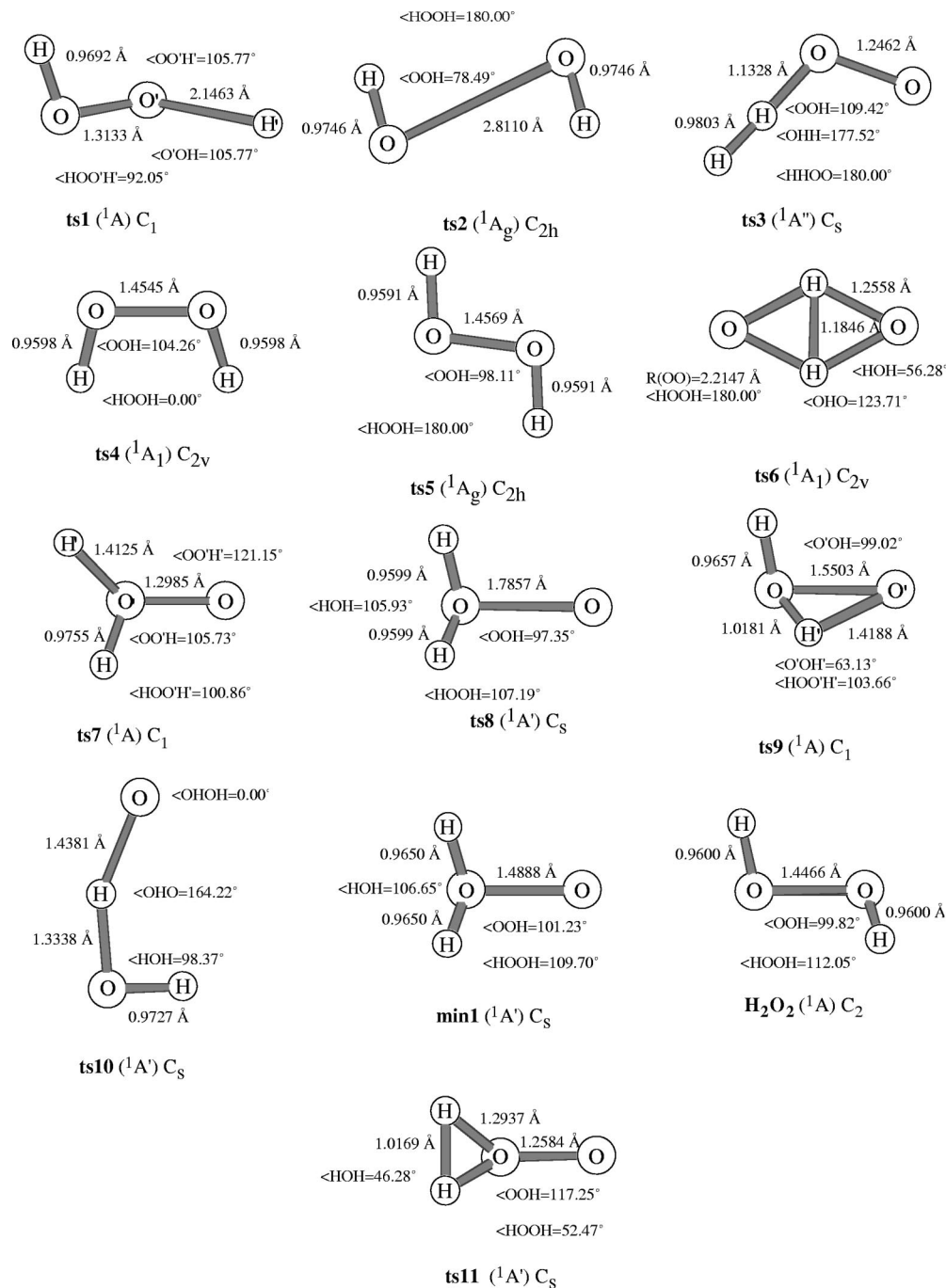
FIG. 1. Stationary points of the PES at the UMP2(FC)/6-311G($3d2f$,$3p2d$) level of calculation, except for the saddle point ts1 which is given at the UMP2(FC)/6-311G(d,p) level. ts11 corresponds to a second order saddle point. See the text.

using the UMP2(FC) method and for all basis sets considered, i.e., 6-311G(d,p), 6-311G($2df$,$2pd$), and 6-311G($3d2f$,$3p2d$). At the PUMP2(FC) level and for all basis sets [with the only exception of ts2 for the 6-311G(d,p) basis set] and at the highest level of the calculation, the PUMP4(FU)//UMP2(FC)/6-311G($3d2f$,$3p2d$) method, however, ts8 and ts2 become energetically below reactants and products, respectively. Because of this we have only considered in the fitting (Sec. II B) three stationary points between reactants and products for the insertion mechanism of reaction (1): min1, ts9, and H$_2$O$_2$, all of them placed energetically below reactants (Fig. 2). Reaction (1)

can also occur according to a second reaction pathway (abstraction microscopic mechanism). Thus, a saddle point (ts10) responsible for the abstraction of an H atom of the H$_2$O molecule by the attacking O(^1D) atom to give two OH radicals has been found. This saddle point leads to an energy barrier of 10.92 kcal mol^{-1}.

The absence of any energy barrier above reactants along the minimum energy path of reaction (1) predicted by the *ab initio* calculations is consistent with the nonexistence of an experimental activation energy.[4] Thus, within the temperature range for which experimental data are available (T = 200– 350 K), the rate constant is independent of the
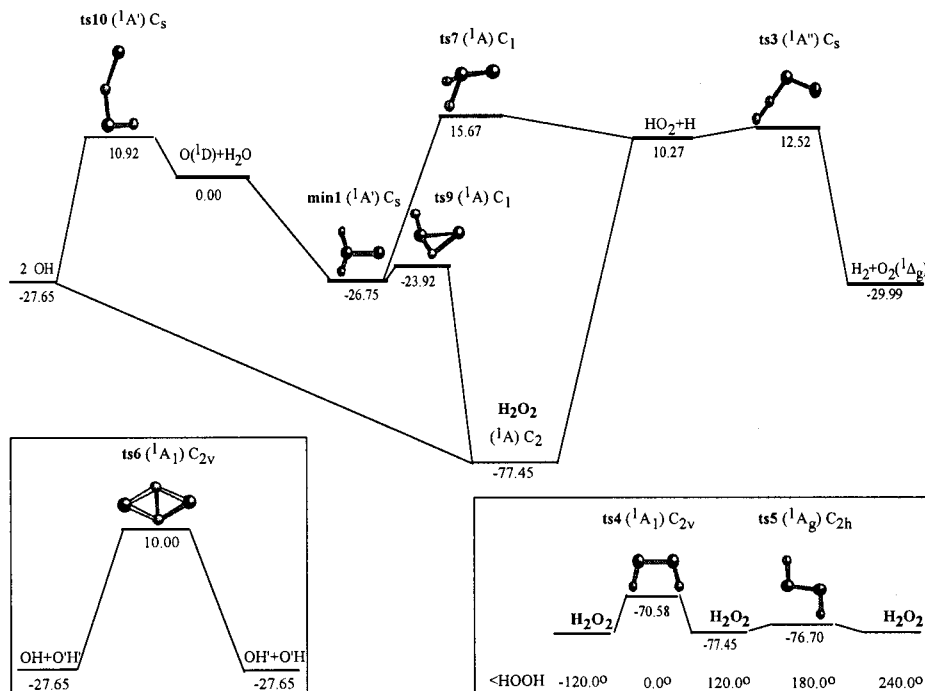
FIG. 2. Energy diagram of the PES at the PUMP4(FU)//UMP2(FC)/ 6-311G($3d2f,3p2d$) level of calculation, including the UMP2(FC)/ 6-311G($3d2f,3p2d$) zero-point energy, referred to reactants (in kcal mol^{-1}).

temperature.[4] The *ab initio* equilibrium geometry of the H$_2$O$_2$ hydrogen peroxide is very close to the experimental one [R(OO)$= 1.4556$ Å, R(OH)$= 0.967$ Å, $<$(OOH) $= 102.32°$, and $<$(HOOH)$= 113.70°$].[27] The agreement with experiments is good and very good in the case of the harmonic frequencies (Table II) and energy (Table I), respectively. The isomerization of H$_2$O$_2$ through ts9 to give min1 was previously described in the context of a CCSD(T) *ab initio* study [coupled-cluster approach including single and double excitations (CCSD) with connected triple excitations].[19] In that work the TZ2P+f and DZP basis sets were used for geometry optimizations and harmonic frequency calculations. But, for the harmonic frequency calculations of ts9 and H$_2$O$_2$ the CCSD method was used instead of the CCSD(T) one. The geometries and harmonic frequencies of min1, ts9, and H$_2$O$_2$ reported here are quite similar to those given in Ref. 19. The barrier for isomerization from min1 to H$_2$O$_2$ obtained here (2.83 kcal mol^{-1}) is also quite close to that reported in Ref. 19 (3.2 kcal mol^{-1}). A saddle point similar to ts2 has been reported previously at the MRCI-SD level [multireference, single, and doubles, configuration interaction (CI) calculation],[21] where the main differences are the $<$(HOOH) dihedral angle (143° [21] vs 180.0° in our case) and the $<$(OOH) angle (59° [21] vs 78.5° in our case).

For reaction (2) only a stationary point (ts11) with two imaginary frequencies that connects min1 with the H$_2$+O$_2$($a\,^1\Delta_g$) products has been found. The difficulties to determine the true saddle point that allows one to connect with products of reaction (2) are probably due to the fact that in this case to evolve from reactants to products two bonds should be formed and two bonds should be removed. This should also involve a significant energy barrier with respect to reactants. The energy barrier associated to the second-order saddle point ts11 (28.3 kcal mol^{-1}) is consistent with

this fact, although, of course, the energy barrier corresponding to the true saddle point must be lower than this value. A saddle point (ts3) which connects these products with the ones of reaction (3) (H+HO$_2$), with an energy of 12.52 kcal mol^{-1} (2.25 kcal mol^{-1} above H+HO$_2$) has also been obtained. The production of H$_2$+O$_2$($a\,^1\Delta_g$) has not been considered in the fitting (Sec. II B), because it is not possible according to the proposed triatomic model (an OH group of the H$_2$O molecule has been taken as a pseudoatom). In fact, while a triatomic model can be used in a QCT study to describe the dynamics of formation of the new OH bond arising from reaction (1), a tetratomic analytical fitting is required to account for the dynamics of reaction (2). Moreover, while it would be possible to compare the dynamics of reaction (1) resulting from triatomic and tetratomic descriptions of the system (that, of course, may be based on the same set of *ab initio* calculations), this would not be the case for reaction (2).

The production of atomic hydrogen and hydroperoxy radical [reaction (3)], as in the case of reaction (1), can also take place along two possible reaction pathways. The first one [insertion microscopic mechanism (via H atom migration)], analogous to that for reaction (1), involves the formation of products when the reactants evolve through the H$_2$O$_2$ hydrogen peroxide minimum [O(^1D)+H$_2$O→ts8→min1 →ts9→H$_2$O$_2$→ts1→H+HO$_2$]. Thus, this reaction path coincides with the corresponding one for reaction (1) until the formation of H$_2$O$_2$. The saddle point ts1 has only been found at the lowest level calculation [UMP2(FC)/6-311G(d,p)]. Thus, the connection between the hydrogen peroxide and products probably take place without the presence of any barrier. Reaction (3) can also occur according to a second pathway (substitution microscopic mechanism). Hence, in this case reaction (3) differs from reaction (1). Thus, a saddle point (ts7) responsible for the evolution from min1 to the

J. Chem. Phys., Vol. 113, No. 16, 22 October 2000

O+H₂O reaction   6741

TABLE II. Harmonic vibrational frequencies (in cm^{-1}) of the stationary points at the UMP2(FC)/6-311G($3d2f,3p2d$) level.

Mode	ts1 C_1[a]	ts2 C_{2h}	ts3 C_s	ts4 C_{2v}	ts5 C_{2h}	ts6 C_{2v}	ts7 C_1
ν_1	3740.1 (A)	3850.0 (B)	1576.9 (A')	3870.7 (A_1)	3873.9 (B_u)	2411.7 (A_1)	3595.2 (A)
ν_2	1455.6 (A)	3693.4 (A)	1506.6 (A')	3829.9 (B_2)	3867.6 (A_g)	1471.0 (B_2)	1420.0 (A)
ν_3	1215.3 (A)	504.5 (A)	1400.7 (A')	1449.8 (B_2)	1532.2 (A_g)	1211.4 (A_1)	1332.9 (A)
ν_4	301.6 (A)	419.4 (B)	854.9 (A'')	1360.0 (A_1)	1248.3 (B_u)	815.7 (B_1)	1049.4 (A)
ν_5	287.6 (A)	262.6 (A)	441.8 (A')	929.6 (A_1)	937.3 (A_g)	760.0 (A_1)	808.7 (A)
ν_6	356.9i (A)	323.7i (A)	3213.7i (A')	596.5i (A_2)	321.3i (A_u)	2337.7i (B_2)	2631.7i (A)

Mode	ts8 C_s	ts9 C_1	ts10 C_s	ts11 C_s	min1 C_s	H₂O₂ C_2[b] Ab initio	Experimental
ν_1	3932.0 (A'')	3786.0 (A)	3734.8 (A')	2286.5 (A')	3836.0 (A'')	3845.3 (A)	3609.8^c
ν_2	3825.6 (A')	3166.3 (A)	1471.1 (A')	1531.3 (A')	3742.8 (A')	3842.3 (B)	3610.7^d
ν_3	1614.8 (A')	1444.4 (A)	1071.2 (A'')	1216.1 (A'')	1615.1 (A')	1438.7 (A)	1395.9^e
ν_4	564.9 (A'')	1011.1 (A)	599.0 (A')	1039.4 (A')	960.4 (A')	1331.4 (B)	1264.6^e
ν_5	558.8 (A')	848.4 (A)	417.8 (A')	1126.9i (A'')	927.0 (A'')	935.4 (A)	865.9^f
ν_6	516.7i (A')	1266.2i (A)	1257.9i (A')	2130.1i (A')	779.7 (A')	401.2 (A)	<400^g

[a]UMP2(FC)/6-311G(d,p) level.
[b]From higher to lower frequencies we have (*ab initio* ordering): OH sym. stretching, OH antisym. stretching, OOH sym. bending, OOH antisym. bending, OO stretching, and torsion.
[c]Reference 28.
[d]Reference 29.
[e]Reference 30.
[f]Reference 31.
[g]Reference 32.

hydroperoxy radical has been found with an energy of 15.67 kcal mol^{-1}.

In Fig. 2 are also included other saddle points (ts4 and ts5) which are associated with the internal rotation of the hydrogen peroxide molecule; ts4 has a dihedral angle of 0° (*cis* arrangement) and ts5 has a dihedral angle of 180° (*trans* arrangement). The saddle point ts4 has a larger energy than ts5 because two different repulsive interactions are possible in the *cis* geometry: one between the oxygen lone pair electrons and the other one between the OH bond dipole moments. In the *trans* geometry (ts5) only the first repulsive interaction is possible. The calculated barriers for the internal rotation of H₂O₂ are 7.38 kcal mol^{-1} (*cis*) and 1.23 kcal mol^{-1} (*trans*), both without including the ZPE. These values compare very well with the experimental data: 7.11 kcal mol^{-1} (*cis*) and 1.10 kcal mol^{-1} (*trans*);[33] 7.33 kcal mol^{-1} (*cis*) and 1.11 kcal mol^{-1} (*trans*).[34]

The saddle point (ts6) of the exchange process of the two hydrogen atoms between the two hydroxyl radicals (ts6) has also been located; it is a quite symmetric (C_{2v}) and energetic saddle point (Fig. 2).

Similar stationary points to those described above for the O(^1D)+H₂O ground PES have been found at the UMP2(FU)/6-31G(d) level for the related O(^1D)+H₂S system.[35] However, at this point it is worth noting that, as indicated at the beginning of this section, the UMP2 geometries of open-shell singlet stationary points, due to spin contamination, are probably located between the singlet and triplet ones. In the O(^1D)+H₂O system, with the exception of min1, ts9, H₂O₂, ts4, and ts5, which have closed-shell character ($\langle S^2 \rangle/\hbar^2 = 0.00$), the stationary points placed between reactants and products have open-shell character ($\langle S^2 \rangle/\hbar^2 = 0.8-1.0$), this fact being a bit more evident for ts10. From preliminary complete active space self-consistent field

(CASSCF) calculations that are in progress in our group, it turns out that the structures reported in the present work are quite similar to the CASSCF ones, with the only exception being what happens for ts10. Thus, at the CASSCF level this stationary point is closer (in geometry and energy) to reactants than in the case of the UMP2 level.

B. Analytical potential energy surface

A triatomic model, where an OH fragment of the H₂O molecule has been treated as a single atom (OH) of 17 amu placed in its center of mass, has been considered to obtain an analytical representation of the ground PES. This model has been suggested from the experimental data, which clearly show that most of the internal energy excitation is channeled towards the OH molecule arising from the new OH bond. This kind of modeling has been previously used in our group in the case of the O(^1D)+CH₄[36] and O(^3P)+CH₄[37] reactions with quite good results.

The same type of analytical expression (many-body expansion[38]) and programs[39,40] used in previous works of our group [e.g., N(^4S)+NO,[41] O(^3P)+CS,[42] H(^2S)+Cl₂, and Cl(^2P)+HCl,[43] N(^4S)+O₂,[44] H+ClF, and F+HCl,[45] O(^1D)+CH₄ (triatomic model),[36] and O(^3P)+CH₄ (triatomic model)[37]] have also been employed here. According to this approach, for the present system the analytical PES can be represented as follows:

$$V(R_1,R_2,R_3) = V^{(2)}_{OH}(R_1) + V^{(2)}_{H(OH)}(R_2) + V^{(2)}_{O(OH)}(R_3)$$
$$+ V^{(3)}_{OH(OH)}(R_1,R_2,R_3), \quad (4)$$

where $V^{(2)}$ and $V^{(3)}$ are the two-body and three-body terms, respectively, and R_1, R_2, R_3 are the O–H, H–(OH), and O–(OH) distances, respectively.

TABLE III. Optimal parameters of the analytical triatomic PES1 and PES2.

Two-body terms:[a]

Species	$a_1/\text{Å}^{-1}$	$a_2/\text{Å}^{-2}$	$a_3/\text{Å}^{-3}$
O–H	3.803 70	3.638 38	3.893 20
H–(OH)	4.693 62	6.154 12	5.645 13
O–(OH)	3.439 69	1.009 98	4.689 48

Three-body term:[b]

	PES1	PES2		PES1	PES2		PES1	PES2
c_{000}	5.417 90	5.247 91	c_{300}	0.230 83	0.420 50	γ_1	0.988 58	1.281 67
c_{100}	0.023 52	0.096 16	c_{210}	−0.740 06	−0.542 62	γ_2	2.367 14	1.979 54
c_{010}	0.045 64	−0.389 97	c_{201}	−0.667 44	−0.320 26	γ_3	2.166 89	1.863 44
c_{001}	1.035 84	0.627 87	c_{120}	−0.696 16	−1.206 22			
c_{200}	0.059 73	0.138 72	c_{111}	3.145 47	2.757 27			
c_{110}	0.876 22	0.526 08	c_{102}	−0.131 92	−0.277 85	R_{OH}^0	1.4427	
c_{101}	1.003 94	0.756 06	c_{030}	1.074 24	1.425 37			
c_{020}	0.591 53	0.179 15	c_{021}	−0.528 41	−0.210 71	$R_{\text{H–(OH)}}^0$	1.4350	
c_{011}	1.443 97	0.867 75	c_{012}	−0.391 98	−0.709 69			
c_{002}	2.541 23	1.819 13	c_{003}	−0.490 54	−0.422 84	$R_{\text{O–(OH)}}^0$	1.4791	

[a]The dissociation energies and equilibrium distances used in the fitting are given in Table IV.
[b]Units are: $c_{ijk}/\text{eV Å}^{-(i+j+k)}$, $\gamma_i/\text{Å}^{-1}$, $R_i/\text{Å}$.

The three asymptotic channels of the ground PES which can be described by the triatomic model [O(^1D)+H$_2$O, OH+OH, and H+HO$_2$, involved in reactions (1) and (3)] do not correlate with the same electronic state of the oxygen atom. Thus, reactants correlate with the first excited state of the O atom [O(^1D)], while the products of reactions (1) and (3) correlate with the ground state of the O atom [O(^3P)]. Because of this, a modified form of the usual many-body equation (4), including a monoatomic term $V^{(1)}$ with a switching function should be used.[38] Although this is a quite well known fact, it was not indicated accurately enough in the text. Of course, this improvement does not affect the contents of the paper at all. Nevertheless, this modification can be avoided if in the fitting of the two-body terms (diatomic potential energy curves) the dissociation limits of those molecules that correlate with O(^3P) are modified so as to reproduce ''artificial'' dissociation limits leading to O(^1D). This approximation only changes the high energy part of the diatomic curve, and the low and moderate energy regions explored in most usual dynamical calculations remain almost unaltered. Hence, analogously as it was done previously by our group in the case of the O(^1D)+CH$_4$ reaction,[36] here we have used modified dissociation energy values for the OH and O(OH) molecules by summing up the O(^1D)-O(^3P) energy difference to the corresponding values describing the dissociation up to O(^3P).

The diatomic potential energy curves have been fitted using the extended-Rydberg potential up to third order

$$V^{(2)}(\rho) = -D_e(1+a_1\rho+a_2\rho^2+a_3\rho^3)e^{-a_1\rho}, \qquad (5)$$

where D_e and R_e are the dissociation energy [altered for OH and O(OH) as it was stated above] and equilibrium bond length of the corresponding diatomic or pseudodiatomic molecule, respectively, and ρ is defined as being equal to $R-R_e$. The optimal $\{a_i\}$ diatomic parameters have been obtained for each molecule using a nonlinear least-squares procedure,[39] by fitting a set of diatomic or pseudodiatomic *ab initio* points calculated around the equilibrium distance

[PUMP4(FU)//UMP2(FC) level]. For the X–(OH) molecules (X=H, O) the OH *ab initio* geometry was optimized in all points of the X–(OH) pseudodiatomic curve. The extended-Rydberg function provides a very good fitting of the curves in all cases. The optimal diatomic parameters of the OH, H(OH), and O(OH) molecules are shown in Table III, and the spectroscopic constants derived from them are given in Table IV.

The three-body term consists of a third-order polynomial, $P(\rho_1,\rho_2,\rho_3)$, multiplied by a range function, $T(\rho_1,\rho_2,\rho_3)$. The polynomial is expressed in terms of three internal coordinates (ρ_1,ρ_2,ρ_3), defined as $\rho_i=R_i-R_i^o$, where the selected reference structure (R_1^o,R_2^o,R_3^o) corresponds to the average pseudotriatomic structure resulting from the two minima of the PES placed between reactants and products (min1 and H$_2$O$_2$). The range function cancels the three-body term as one of the three atoms is separated from the other two. Thus, we have

$$V_{\text{OH(OH)}}^{(3)}(\rho_1,\rho_2,\rho_3)=P(\rho_1,\rho_2,\rho_3)T(\rho_1,\rho_2,\rho_3), \qquad (6)$$

where

$$P(\rho_1,\rho_2,\rho_3) = \sum_{i,j,k=0}^{0\leq i+j+k\leq 3} c_{ijk}\rho_1^i\rho_2^j\rho_3^k, \qquad (7)$$

with i, j, and k being positive integer numbers, and

$$T(\rho_1,\rho_2,\rho_3) = \prod_{i=1}^{3}\left[1-\tanh\left(\frac{\gamma_i\rho_i}{2}\right)\right]. \qquad (8)$$

The 20 linear parameters ($\{c_{ijk}\}$ polynomial coefficients) and three nonlinear ones ($\{\gamma_i\}$ range function parameters) of the three-body term have been determined by a weighted nonlinear least-squares procedure,[40] taking into account the three *ab initio* saddle points (ts7, ts9, and ts10), the two minima (min1 and H$_2$O$_2$), and 113 additional points corresponding to the connections between the different stationary points of the ground ^1A PES:O(^1D)+H(OH)→OH+(OH) (abstraction) (24 points); O(^1D)+H(OH)→H+O(OH) (sub-

TABLE IV. Spectroscopic constants of the diatomic and pseudodiatomic molecules.

Species	D_e^a/eV	R_e^b/Å	ν_e/cm^{-1}	$\nu_e x_e$/cm^{-1}	B_e/cm^{-1}	α_e/cm^{-1}
O–H						
Analytical fit	6.7233	0.9666	3723.8	73.16	19.03	0.7337
Experimental[c]	6.587	0.969 66	3737.76$_1$	84.881$_3$	18.910$_8$	0.7242
H–(OH)						
Analytical fit	5.4399	0.9721	3887.7	71.29	18.75	0.6755
Experimental	5.443^d	0.9736^f				
O–(OH)						
Analytical fit	4.9602	1.323 2	1267.0	17.52	1.168	0.0193
Experimental	5.00^e	1.345 8^f				

^{a}*Ab initio* and experimental D_e for O–H and O–(OH) have been modified by summing up the experimental O(^1D)–O(^3P) energy difference (1.966 eV) (Ref. 46). The PUMP4(FC)/6-311G($3d2\,f$,$3p2d$) O(^1D)–O(^3P) energy difference is 1.901 eV.
^{b}Equilibrium distances for the pseudodiatomic: H–(OH) and O–(OH) molecules correspond to the distances between the atom and the pseudoatom (OH) center of mass.
^{c}Reference 47.
^{d}From D_0(H–OH) (Ref. 48) and taking into account the harmonic frequencies of H$_2$O (Ref. 48) and OH (Ref. 47).
^{e}From D_0(O–OH) assumed to be approximately equal to ΔH_{0K}^0 of the HO$_2$→OH+O dissociation process (Ref. 3) and taking into account the harmonic frequencies of HO$_2$ (Ref. 49) and OH (Ref. 47).
^{f}Reference 27.

stitution) (42 points); O(^1D)+H(OH)→HO(OH) (hydrogen peroxide minimum)→OH+(OH), H+O(OH) (insertion mechanism) (47 points). In the fitting procedure different weights were used for each one of these regions and for the first partial potential energy derivatives (equal to zero) at the saddle points and minima geometries with respect to the R$_{OH}$ and R$_{H(OH)}$ distances and <(OH(OH)) angle. The optimal three-body parameters and the properties of the saddle points and minima of the two analytical expressions selected (PES1 and PES2) are given in Tables III and V, respectively.

The root-mean-square deviation (RMSD) for the 118 *ab initio* points fitted is equal to 0.1054 eV (2.43 kcal mol^{-1}) for PES1 and 0.0944 eV (2.18 kcal mol^{-1}) for PES2. Overall there is a reasonably good agreement between the *ab initio*

properties of the stationary points and those resulting from the fitting, except for the saddle point ts10 (Table V). Both analytical PES give a ts10 with an <(OH(OH)) angle of 180° and a barrier much smaller than the *ab initio* one. We have tried to improve this result including the bending of ts10, but although we have obtained an improvement in the description of ts10, with an <(OH(OH)) angle of 169° and a higher energy (9.65 kcal mol^{-1} without including the ZPE), the description of min1 and H$_2$O$_2$ was quite unsatisfactory. Nevertheless, in this context (triatomic modeling), which can be considered as a starting point for the dynamics study of this reaction, the optimal analytical expressions obtained (PES1 and PES2) can be considered as an acceptable representation of the quite complicated ground PES. As it will be

TABLE V. Properties of the fitted stationary points for the analytical triatomic PES1 and PES2.^{a}

Stationary point^b	$R_{O-(OH)}$/Å	R_{O-H}/Å	$R_{H-(OH)}$/Å	∠O–(OH)–H/°	∠O–H–(OH)/°	E/kcal mol^{-1}	E+ZPE/kcal mol^{-1}	ν_i/cm^{-1}
ts7 (C_s)								
ab initio	1.3153	2.3620	1.4145	119.78	28.90	17.57	15.67	
PES1	1.2793	2.8942	2.2135	108.96	24.71	12.03	9.11	398.5i, 362.8, 1483.5
PES2	1.3167	3.9480	3.2200	114.26	17.70	11.16	7.55	92.9i, 98.5, 1266.1
ts9 (C_s)								
ab initio	1.5602	1.4188	1.0354	62.47	77.20	−24.95	−23.92	
PES1	1.4911	1.5054	1.0940	69.29	67.89	−27.20	−27.32	1225.7i, 2874.8, 932.2
PES2	1.5085	1.4857	1.1029	67.29	69.49	−26.14	−27.00	1476.4i, 2458.1, 832.5
ts10 ($C_{\infty v}$)								
ab initio	2.7128	1.4381	1.3512	13.89	153.08	14.2	10.92	
PES1	2.5554	1.4668	1.0886	0.00	180.00	2.44	0.74	1151.8i, 1065.2(2), 569.1
PES2	2.5850	1.4630	1.1220	0.00	180.00	4.09	1.71	1587.8i, 861.1(2), 499.3
min1 (C_s)								
ab initio	1.5009	1.9254	0.9827	99.54	50.24	−30.08	−26.75	
PES1	1.5944	1.9358	0.8936	95.72	54.61	−33.22	−30.02	4442.3, 976.04, 707.9
PES2	1.5722	1.8587	0.8902	92.71	57.56	−33.73	−30.70	4177.5, 1035.3, 798.1
H$_2$O(C_s)^c								
ab initio	1.4573	0.9600	1.8872	30.00	49.37	−80.68	−77.45	
PES1	1.4465	0.9502	1.8839	29.61	48.77	−80.85	−78.16	3834.4, 1059.6, 874.4
PES2	1.4646	0.9595	1.7888	32.40	54.87	−81.82	−78.65	3678.1, 1556.7, 871.2

^{a}Energy referred to reactants.
^{b}For each stationary point the *ab initio* triatomic symmetry point group is indicated.
^{c}The H–O–(OH) angle for H$_2$O$_2$ is: 100.63, 101.62, and 92.73 for *ab initio*, PES1, and PES2, respectively.

seen in Sec. III, in spite of the low energy barrier that ts10 presents in both analytical PES considered, at the moderate collision energies considered in this work nearly all reactive trajectories evolve through geometrical arrangements close to that of the HO(OH) hydrogen peroxide minimum. This means that the dominant microscopic mechanism clearly corresponds to the insertion process, the abstraction process through the saddle point ts10 playing a minor role.

III. QCT DYNAMICS CALCULATIONS

To study the dynamics of reaction (1) the QCT method[50–52] has been applied as implemented in the TRIQCT program,[53] considering the PES1 and PES2 triatomic analytical representations of the ground ^1A PES. The accuracy of the numerical integration of Hamilton's differential equations has been verified by checking the conservation of total energy and angular momentum along every trajectory, and performing back integrations on some batches of trajectories. An integration step of 2.5×10^{-17} s and an initial distance of 10 Å between the $O(^1D)$ atom and the H–(OH) center of mass have been selected. At this separation the reactants interaction energy can be neglected with respect to the reactants available energy.

The QCT dynamics study has been mainly focused on the calculation of the rovibrational distributions of the OH product from reaction (1) and the corresponding microscopic reaction mechanism, although other properties have also been considered (rate constant and rotational alignment). The reported experimental OH rovibrational distributions arising from reaction (1) correspond to several reaction conditions, concerning mostly the identity of the $O(^1D)$ precursor and the wavelength used in its photodissociation. The different conditions yield, in turn, different relative translational energy (collision energy) distributions for $O(^1D) + H_2O$. In the QCT calculations three different relative translational energies (E_T) for the $O(^1D) + H_2O$ system have been explored: (a) $E_T = 0.443$ eV ($\langle E_T \rangle$ from N_2O photodissociation at 193 nm); (b) $E_T = 0.303$ eV ($\langle E_T \rangle$ from O_3 photodissociation at 248 nm); (c) $E_T = 0.234$ eV ($\langle E_T \rangle$ from O_3 photodissociation at 266 nm). In these calculations the rovibrational distribution of the H–(OH) pseudodiatomic molecule has been sampled from a Maxwell–Boltzmann distribution at 300 K. Both the collision energy and the H–(OH) rovibrational levels have been sampled from Maxwell–Boltzmann distributions at 300 K in the rate constant calculation of reaction (1). For each initial condition around 10 000 trajectories have been run.

A. Rate constant and rovibrational distributions

The QCT reaction cross section (σ) of $O(^1D) + H-(OH)(300 \text{ K}) \rightarrow OH + (OH)$ has been calculated at the three E_T values explored for the two triatomic analytical PES derived. σ decreases with E_T, as it corresponds for a barrierless reaction (e.g., for PES1 $\sigma = 26.4$, 21.2, and 16.0 Å^2 for $E_T = 0.234$, 0.303, and 0.443 eV, respectively). This behavior is due to the decrease of the maximum impact parameter (b_{max}) with E_T, the reaction probability being almost constant (around 50%). A large amount of energy is released as OH internal energy, appearing in very similar energy

amounts as vibration and rotation. For PES1 at 0.303 eV, the average fraction of energy appearing in products as relative translation ($\langle f'_T \rangle$), vibration ($\langle f'_V \rangle$), and rotation ($\langle f'_R \rangle$) is equal to 0.29, 0.34, and 0.38, respectively.

The QCT rate constant of reaction (1) at 300 K has been estimated from the rate constant obtained for the ground PES ($^1A'$ in C_s) by dividing its value by five, as there are five degenerated PES in the reactants region (four of them correlating with products). Hence, in the absence of additional information on the excited PES of the $O(^1D) + H_2O$ system, we are assuming that the reactivity is dominated by the ground PES. The rate constant of reaction (1) estimated from the QCT calculations is reasonably close to the recommended experimental value, 2.2 $(-0.45, +0.57)$ 10^{-10} cm^3 molecule^{-1} s^{-1},[4] in the case of PES1 $[(1.32 \pm 0.01)$ 10^{-10} cm^3 molecule^{-1} s^{-1} while it is considerably lower in the case of PES2 $[(0.51 \pm 0.01)$ 10^{-10} cm^3 molecule^{-1} s$^{-1}]$. Contributions of the excited PES [especially the first $^1A''(C_s)$] would tend to increase the calculated rate constant and a better agreement with the experimental value could be expected.

The QCT OH vibrational distributions and average rotational energies, corresponding to the new OH bond formed, obtained for the above-mentioned E_T values [H–(OH) molecule at 300 K] together with the experimental data available are given in Table VI. From the QCT results it turns out that OH vibrational levels up to $v' = 4$ are populated, and the vibrational populations decrease with v' [e.g., for PES1 at $E_T = 0.303$ eV, $P(v'=0):P(v'=1):P(v'=2):P(v'=3):P(v'=4) = 1.00:0.65:0.34:0.16:0.01]$. The average rotational energy of each OH vibrational level increases with E_T, and the OH rotational energy content decreases with the OH vibrational energy, as expected. Overall, the QCT vibrational populations for $v' = 0-2$ are in good agreement with the experimental values reported for the OH which corresponds to the new OH bond formed,[6,7,10,11,15] which is substantially more excited than that associated with the old one. For $v' = 3$ and 4, however, there is no experimental information available. The QCT OH average rotational energies obtained are in general much larger than the experimental ones for the new OH bond.[6,7,10,11,15]

B. Two-vector properties and microscopic reaction mechanism

An $\mathbf{l} \rightarrow \mathbf{l'}$ angular momentum transformation has been found, with $\mathbf{l}(\mathbf{l'})$ being the reactants (products) orbital angular momentum. This is what can be expected for a reaction with $\mathbf{H}-\mathbf{L}-\mathbf{H}$ (heavy–light–heavy) kinematics. In what respects the two-vector properties, the angular distribution (reactive trajectories vs scattering angle) is very broad and presents a somewhat larger tendency towards forward scattering, the forward/backward (f/b) ratio being higher than unity in all cases. The f/b ratio increases with E_T (e.g., for PES1 f/b = 1.09, 1.16, and 1.30 at $E_T = 0.234$, 0.303, and 0.443 eV, respectively), and the initial ($\mathbf{k}$) and final ($\mathbf{k'}$) relative velocity vectors exhibit an average angle of about 90° in all cases. The OH rotational angular momentum ($\mathbf{j'}$) has some tendency to be perpendicular to $\mathbf{k}$ and $\mathbf{k'}$, and the $\mathbf{kj'}$ and $\mathbf{k'j'}$ angular distributions are very similar (broad,

TABLE VI. Vibrational populations and average rotational energy (kcal mol^{-1}) of the OH molecules arising from the O(^1D)+H$_2$O→2 OH reaction.[a,b]

	P_1/P_0 ($\langle E'_R\rangle_{v'=0}$)	P_2/P_1 ($\langle E'_R\rangle_{v'=1}$)	P_3/P_2 ($\langle E'_R\rangle_{v'=2}$)	P_4/P_3 ($\langle E'_R\rangle_{v'=3}$)
N$_2$O 193 nm				
QCT PES1	0.69 (23.8)	0.60 (17.6)	0.57 (12.3)	0.16 (5.9)
QCT PES2	0.76 (25.7)	0.64 (19.5)	0.67 (12.4)	0.16 (6.2)
Experiment[c]	0.68 (11.9)	··· (4.4)		
O$_3$ 248 nm				
QCT PES1	0.65 (22.6)	0.53 (16.7)	0.46 (10.7)	0.07 (4.1)
QCT PES2	0.71 (24.5)	0.63 (17.1)	0.54 (10.3)	0.10 (4.5)
Experiment[d]	1.08±0.10 (38.8)	0.50±0.10 (9.1)		
O$_3$ 266 nm				
QCT PES1	0.58 (23.5)	0.55 (14.9)	0.37 (9.5)	0.03 (3.3)
QCT PES2	0.68 (23.6)	0.58 (15.0)	0.50 (9.3)	0.03 (3.0)
Experiment[e]	0.63±0.18 (9.1)	··· (7.9)		
Experiment[f]	0.78 (5.2)	0.50 (3.2)		
Experiment[g]	0.76±0.15 (9.8±0.5)	··· (7.9±0.9)		

[a]QCT results for E_T=0.443 eV (N$_2$O, λ=193 nm), 0.303 eV (O$_3$, λ=248 nm), 0.234 eV (O$_3$, λ=266 nm), and H–(OH) at T=300 K.
[b]The experimental data refer to the OH molecules which correspond to the new OH bond. See the text.
[c]Reference 14. $T_R(v'=0)$=6000 K; $T_R(v'=1)$=2200 K.
[d]Reference 10. $T_R(v'=0)$=600 K (low j') and 19 500 K (high j'); $T_R(v'=1)$=400 K (low j') and 4600 K (high j'). For both vibrational levels the high j' component of the distribution clearly dominates over the low j' one, and the average rotational energies have been derived from them.
[e]Reference 6. $T_R(v'=0)$=4600 K; $T_R(v'=1)$=4000 K.
[f]Reference 7. $T_R(v'=0)$=2600 K; $T_R(v'=1)$=1600 K.
[g]Reference 11. $\langle E'_R\rangle_{v'=0}$=3440±160 cm^{-1}; $\langle E'_R\rangle_{v'=1}$=2780±300 cm^{-1}.

peaking at 90°, and symmetrical around 90°). The **l'j'** angular distribution is broad and both vectors show a slight tendency to be antiparallel, with an average angle between 102° and 106°.

At E_T=0.234 eV, the QCT value of $\langle P_2(\cos\theta)\rangle$ for **kj'**, defined as $\langle 3\cos^2\theta-1\rangle/2$, with θ being the angle defined by **k** and **j'**, is equal to −0.0106 and −0.0155 for PES1 and PES2, respectively, and these values compare well with the experiment (0.14±0.22).[11] $P_2(\cos\theta)$ presents the following range of values: $-0.5\leq P_2(\cos\theta)\leq 1.0$, where −0.5 (1.0) corresponds to **j'** perpendicular (parallel) to **k**. Hence, for reaction (1) there is no clear tendency to a particular rotational alignment of the OH product with respect to the initial relative velocity vector. The situation for **k'j'** is very similar to that for **kj'**. Thus, the associated $\langle P_2(\cos\theta)\rangle$ value is equal to −0.0099 and −0.0080 for PES1 and PES2, respectively.

For PES1, the consideration of the reactive trajectories obtained (4475) at E_T=0.303 eV has allowed the study of the microscopic mechanism of reaction (1). The lowest potential energy reached on PES1 by each reactive trajectory has been analyzed. For PES1, the energy of reactants, OH+(OH) products and HO(OH) hydrogen peroxide minimum are: −5.44, −6.72, and −8.95 eV, respectively. Only 1.8% of reactive trajectories have evolved from reactants to products with a lowest potential energy higher than −7.0 eV. The lowest potential energy values reached by the remaining reactive trajectories are the following: 0.4% between −7.0 and −8.0 eV, 1.7% between −8.0 and −8.4 eV, 46.8% between −8.4 and −8.9 eV, and 49.3% below −8.9 eV. Similar results have been obtained for PES2. Hence, the HO(OH) deep minimum plays a very important role in the dynamics, since nearly all reactive trajectories leading to OH+(OH) evolve through geometries close to this minimum. Therefore,

reaction (1) takes place nearly exclusively through an insertion mechanism instead of by abstraction of the H atom by the attacking O(^1D) atom.

To complete the microscopic mechanism analysis, the collision complex lifetimes, τ_C, has been determined for the reactive trajectories (4379) leading to OH+(OH) products on PES1 at E_T=0.443 eV, the highest collision energy considered, and these values have been compared with the average rotational period ($\langle\tau_R\rangle$=0.18 ps) estimated according to this expression

$$\langle\tau_R\rangle\simeq\frac{2\pi\langle I\rangle}{(2\mu E_T)^{1/2}\langle b\rangle}, \qquad (9)$$

where $\langle I\rangle$ is the moment of inertia of the collision complex, which has been taken to be equal to an average over the principal moments of inertia of the HO(OH) hydrogen peroxide minimum at its equilibrium geometry, μ is the reduced mass of reactants, and $\langle b\rangle$ is the average impact parameter.

Although, as indicated above, nearly all reactive trajectories evolve through an insertion mechanism involving the HO(OH) minimum, the analysis of the τ_C values for the above-mentioned condition reveals that reactive trajectories leading to OH+(OH) can be classified into three groups: (a) direct reactive trajectories (30%); (b) nondirect reactive trajectories involving short-lived collision complexes, i.e., those collision complexes with lifetimes shorter than a rotational period (15%), 0.025 ps$<\tau_C<$0.18 ps ($\langle\tau_C\rangle$ =0.091 ps); (c) nondirect reactive trajectories involving long-lived collision complexes, i.e., those collision complexes with lifetimes larger than a rotational period (55%), $\tau_C>$0.18 ps ($\langle\tau_C\rangle$=0.65 ps). Hence, the global average lifetime of the collision complex is 0.53 ps, about three times the rotational period of the HO(OH). For τ_C values of about 0.025 ps there is a temporal gap which suggests the defini-

tion of the border line between direct and nondirect reactive trajectories at 0.025 ps. The QCT average lifetime values obtained must be considered as a lower limit of the theoretical value which would result after including explicitly all degrees of freedom of the H_2O molecule.

The QCT results show that, even at the highest E_T value explored, nearly all reactive trajectories leading to reaction (1) take place through an insertion mechanism which is mainly (70%) a nondirect one. The HO(OH) collision complex formation with an average lifetime of about three rotational periods is consistent with the experimental information available.[10,11,16] Moreover, the highly asymmetrical energy partitioning between the two OH fragments arising from reaction (1) experimentally found,[6,7,10,11,15] indicates that the energy equidistribution between both OH fragments in the collision complex cannot take place within the time scale of only a few rotational periods.

IV. SUMMARY AND CONCLUDING REMARKS

An *ab initio* study of the ground potential energy surface (^1A) of the $O(^1D) + H_2O$ system has been performed, employing the second- and fourth-order Møller–Plesset methods and mainly using the 6-311G($3d2f$,$3p2d$) basis set. Reactants, products, ten saddle points, and two minima, one of them corresponding to the hydrogen peroxide molecule, have been characterized. The ground PES has been modeled as a triatomic system, with an OH group of the H_2O molecule treated as a single atom of 17.0 amu. This model has been suggested from the experimental data. From the PES stationary points and more than one hundred additional points calculated, two triatomic analytical PES models (PES1 and PES2) have been derived using as analytical expression a many-body expansion. Both analytical PES have been employed quite satisfactorily to study the dynamics of reaction (1) by means of the quasiclassical trajectory (QCT) method. In general, PES1 provides a slightly better description of the *ab initio* data and dynamics than PES2.

The QCT dynamics study has been mainly focused on the determination of properties for which experimental data are available. The rate constant of reaction (1) estimated from the QCT calculations is reasonably close to the recommended experimental value in the case of PES1. For E_T = 0.234, 0.303, and 0.443 eV with H_2O at 300 K, overall the QCT OH vibrational populations are in good agreement with the experimental values reported for the OH which corresponds to the new OH bond formed. However, the QCT OH average rotational energies are in general quite larger than the experimental ones for the new OH bond. The QCT values of $\langle P_2(\cos\theta) \rangle$ for **kj**′ at E_T = 0.234 eV compare well with the experiment. Thus, there is not a clear tendency to a particular rotational alignment of the OH product (new OH bond) with respect to the initial relative velocity vector. The QCT results also show that nearly all reactive trajectories leading to reaction (1) take place through insertion microscopic mechanism, which, even at the highest collision energy considered (E_T = 0.443 eV), is mainly (70%) a nondirect one and involves the formation of a collision complex. The collision complex has an average lifetime of about three rotational periods and geometry around that of the HO(OH)

hydrogen peroxide molecule. From this theoretical data, and taking into consideration the highly asymmetrical energy partitioning between the two OH fragments from reaction (1) experimentally found, it turns out that the energy redistribution between the two OH fragments in the collision complex cannot take place in the time scale of only a few rotational periods. The QCT results concerning the microscopic mechanism of reaction (1) are in agreement with the suggestions made by the experimentalists to interpret their results.

The *ab initio*-based QCT triatomic study presented here should be considered as a starting point in the study of the $O(^1D) + H_2O \rightarrow 2OH$ reaction, from which different aspects about the dynamics may be learned. At present, further developments, which take into account explicitly all atoms involved in this tetratomic system, are in progress.

[1] J. R. Wiesenfeld, Acc. Chem. Res. **15**, 110 (1982).

[2] P. Warneck, *Chemistry of the Natural Atmosphere* (Academic, San Diego, 1988).

[3] M. W. Chase, Jr., C. A. Davies, J. R. Downey, Jr., D. J. Frurip, R. A. McDonald, and A. N. Syverud, J. Phys. Chem. Ref. Data Suppl. **14**, 1 (1985).

[4] R. Atkinson, D. L. Baulch, R. A. Cox, R. F. Hampson, Jr., J. A. Kerr, and J. Troe, J. Phys. Chem. Ref. Data **21**, 1125 (1992).

[5] R. Zellner, G. Wagner, and B. Himme, J. Chem. Phys. **84**, 3196 (1980).

[6] J. E. Butler, L. D. Talley, G. K. Smith, and M. C. Lin, J. Chem. Phys. **74**, 4501 (1981).

[7] K.-H. Gericke, F. J. Comes, and R. D. Levine, J. Chem. Phys. **74**, 6106 (1981).

[8] F. J. Comes, K.-H. Gericke, and J. Manz, J. Chem. Phys. **75**, 2853 (1981).

[9] W. A. Guillory, K.-H. Gericke, and F. J. Comes, J. Chem. Phys. **78**, 5993 (1983).

[10] C. B. Cleveland and J. R. Wiesenfeld, J. Chem. Phys. **96**, 248 (1992).

[11] D. G. Sauder, J. C. Stephenson, D. S. King, and M. P. Casassa, J. Chem. Phys. **97**, 952 (1992).

[12] D. S. King, D. G. Sauder, and M. P. Casassa, J. Chem. Phys. **97**, 5919 (1992).

[13] D. S. King, D. G. Sauder, and M. P. Casassa, J. Chem. Phys. **100**, 4200 (1994).

[14] N. Tanaka, M. Takayanagi, and I. Hanazaki, Chem. Phys. Lett. **254**, 40 (1996).

[15] N. Tanaka, U. Nagashima, M. Takayanagi, H. L. Kim, and I. Hanazaki, J. Phys. Chem. A **101**, 507 (1997).

[16] H. Tsurumaki, Y. Fujimura, and O. Kajimoto, J. Chem. Phys. **110**, 7707 (1999).

[17] K. Imura, M. Veneziani, T. Kasai, and R. Naaman, J. Chem. Phys. **111**, 4025 (1999).

[18] L. B. Harding, J. Phys. Chem. **93**, 8004 (1989).

[19] C. Meredith, T. P. Hamilton, and H. F. Schaefer III, J. Phys. Chem. **96**, 9250 (1992).

[20] J. Koput, S. Carter, and N. C. Handy, J. Phys. Chem. A **102**, 6325 (1998).

[21] L. B. Harding, J. Phys. Chem. **95**, 8653 (1991).

[22] M. J. Frisch, G. W. Trucks, H. B. Schlegel, P. M. W. Gill, B. G. Johnson, M. A. Robb, J. R. Cheeseman, T. Keith, G. A. Peterson, J. A. Montgom-

ery *et al.*, GAUSSIAN 94, Revision E. 1, Gaussian, Inc., Pittsburgh, PA, 1995.

[23] K. Stark and H. Werner, J. Chem. Phys. **104**, 6515 (1996).

[24] K. A. Peterson and T. H. Dunning, Jr., J. Phys. Chem. A **101**, 6280 (1997).

[25] W. Chen and H. B. Schlegel, J. Chem. Phys. **101**, 5957 (1994).

[26] R. Caballol, O. Castell, F. Illas, I. P. R. Moreira, and J. P. Malrieu, J. Phys. Chem. A **101**, 7860 (1997).

[27] *Structure Data of Free Polyatomic Molecules*, edited by K. Kuchitsu (Springer, Berlin, 1998), Landolt-Börnstein, Vol. II/25A.

[28] W. B. Olson, R. H. Hunt, B. W. Young, A. G. Maki, and J. W. Brault, J. Mol. Spectrosc. **127**, 12 (1988).

[29] W. B. Cook, R. H. Hunt, W. N. Shelton, and F. A. Flaherty, J. Mol. Spectrosc. **171**, 91 (1995).

[30] A. Perrin, A. Valentin, J.-M. Flaud, C. Camy-Peyret, L. Schriver, A. Schriver, and Ph. Arcas, J. Mol. Spectrosc. **171**, 358 (1995).

[31] C. Camy-Peyret, J.-M. Flaud, J. W. C. Johns, and M. Nöel, J. Mol. Spectrosc. **155**, 84 (1992).

[32] T. Shimanouchi, J. Phys. Chem. Ref. Data **6**, 993 (1977).

[33] J. Koput, J. Mol. Spectrosc. **115**, 438 (1986).

[34] J.-M. Flaud, C. Camy-Peyret, J. W. C. Johns, and B. Carli, J. Chem. Phys. **91**, 1504 (1989).

[35] A. Goumri, J.-D. R. Rocha, D. Laakso, C. E. Smith, and P. Marshall, J. Chem. Phys. **101**, 9405 (1994).

[36] M. González, J. Hernando, I. Baños, and R. Sayós, J. Chem. Phys. **111**, 8913 (1999).

[37] M. González, J. Hernando, J. Millán, and R. Sayós, J. Chem. Phys. **110**, 7326 (1999).

[38] J. N. Murrell, S. Carter, S. C. Farantos, P. Huxley, and A. J. C. Varandas, *Molecular Potential Energy Surfaces* (Wiley, New York, 1984).

[39] M. González and R. Sayós, DIATOMFIT (unpublished program).

[40] R. Sayós and M. González, SM3FIT (unpublished program).

[41] M. Gilibert, A. Aguilar, M. González, F. Mota, and R. Sayós, J. Chem. Phys. **97**, 5542 (1992).

[42] M. González, J. Hijazo, J. J. Novoa, and R. Sayós, J. Chem. Phys. **105**, 10999 (1996).

[43] M. González, J. Hijazo, J. J. Novoa, and R. Sayós, J. Chem. Phys. **108**, 3168 (1998).

[44] R. Sayós, J. Hijazo, M. Gilibert, and M. González, Chem. Phys. Lett. **284**, 101 (1998).

[45] R. Sayós, J. Hernando, J. Hijazo, and M. González, Phys. Chem. Chem. Phys., **1**, 947 (1999).

[46] S. Bashkin and J. O. Stoner, *Atomic Energy Levels and Grotrian Diagrams* (North-Holland, Amsterdam, 1975), Vol. 1.

[47] K. P. Huber and G. Herzberg, *Molecular Spectra and Molecular Structure* (Van Nostrand Reinhold, New York, 1979), Vol. 4.

[48] G. Herzberg, *Molecular Spectra and Molecular Structure* (Van Nostrand Reinhold, New York, 1966), Vol. 3.

[49] M. E. Jacox, ''Vibrational and Electronic Energy Levels of Polyatomic Transient Molecules,'' in: *NIST Chemistry WebBook, NIST Standard Reference Data Base Number 69*, edited by W. G. Mallard and P. J. Linstrom (National Institute of Standards and Technology, Gaithersburg, MD, Feb. 2000) (http://webbook.nist.gov).

[50] R. N. Porter and L. M. Raff, in: *Dynamics of Molecular Collisions*, edited by W. H. Miller (Plenum, New York, 1976), Part B, p. 1.

[51] D. G. Truhlar and J. T. Muckerman, in: *Atom-molecule Collision Theory: A Guide for the Experimentalist*, edited by R. B. Bernstein (Plenum, New York, 1979), p. 505.

[52] H. R. Mayne, Int. Rev. Phys. Chem. **10**, 107 (1991).

[53] R. Sayós and M. González, TRIQCT (unpublished program).